Dipolar bilayer with antiparallel polarization: A self-bound liquid

Martin Hebenstreit,[1,2] Michael Rader,[1,2] and Robert E. Zillich[2,*]
[1]*Institute for Theoretical Physics, University of Innsbruck, Technikerstrasse 21a, 6020 Innsbruck, Austria*
[2]*Institute for Theoretical Physics, Johannes Kepler University, Altenbergerstrasse 69, 4040 Linz, Austria*
(Received 19 December 2014; published 12 January 2016)

Dipolar bilayers with antiparallel polarization, i.e., opposite polarization in the two layers, exhibit liquidlike rather than gaslike behavior. In particular, even without external pressure, a self-bound liquid droplet of constant density will form. We investigate the symmetric case of two identical layers, corresponding to a two-component Bose system with equal partial densities. The zero-temperature equation of state $E(\rho)/N$, where ρ is the total density, has a minimum, with an equilibrium density that can be adjusted by the distance d between the layers (decreasing with increasing d). The attraction necessary for a self-bound liquid comes from the interlayer dipole-dipole interaction that leads to a mediated intralayer attraction. We investigate the regime of negative pressure towards the spinodal instability, where the bilayer is unstable against infinitesimal fluctuations of the total density, confirmed by calculations of the speed of sound of total density fluctuations.

DOI: 10.1103/PhysRevA.93.013611

I. INTRODUCTION

Experiments with Bose gases of atoms with large magnetic moments (^{52}Cr [1,2], ^{164}Dy [3], ^{168}Er [4]) are fueling the interest to understand the effects of the dipole-dipole interaction (DDI) on the stability, shape, and dynamics of dipolar Bose condensates (reviewed in Refs. [5–7]). The strength of the DDI is commonly characterized by the dipole length $r_D = mD^2/(4\pi\varepsilon_0\hbar^2)$, where m is the mass of the dipolar atom or molecule and D is its dipole moment. The value of r_D can be compared with the average interparticle spacing, $r_s \sim \rho^{-1/m}$, where ρ is the number density of the condensate and m is the dimensionality. For $r_D \ll r_s$, the DDI is weak; in general, other contributions to the interaction, such as the s-wave scattering length a, will dominate (except if a is tuned to a sufficiently small value [2]). For $r_D \gtrsim r_s$, the DDI will be the dominant interaction. The magnetic DDI is usually negligible; only for the handful of atoms mentioned above has its effect been observed, as it is difficult to increase the density such that $r_D \gtrsim r_s$. Compared with the magnetic dipole moment of atoms, the electric dipole moment of heteronuclear molecules can be orders of magnitude larger, leading to large values for r_D (e.g., $r_D = 5 \times 10^5$ Å for a fully polarized NaCs). Association of two atoms using a Feshbach resonance and transfer to the rovibrational ground state has been achieved, for example, for ^{7}Li ^{133}Cs [8], ^{40}K ^{87}Rb [9], ^{41}K ^{87}Rb [10], and ^{85}Rb ^{133}Cs [11,12]. But it is quite a challenge to produce a degenerate quantum gas of dipolar molecules.

The anisotropy of the DDI leads to a measurable anisotropy of the speed of sound [13], but an anisotropic superfluid response [14] has also been predicted. The attractive part of the DDI can give rise to roton or rotonlike excitations in a dipolar Bose gas layer [15–19]. An anisotropic 2D quantum gas can be realized by tilting the polarization dipoles in a deep one-dimensional (1D) trap, and a stripe phase can form spontaneously [20,21]. For $r_D \gg r_s$, dipoles will crystallize without imposing an optical lattice [22–25]. Fermionic dipoles in 1D, polarized along the length of the system, can be self-bound, as has been shown using mean-field theory [26]. A bilayered dipolar Bose gas can dimerize if the polarization direction in the two layers is the same [27]. Also, glassy behavior has been studied for antiparallel polarization in two layers, i.e., when dipoles are perpendicular to the layer, but the orientation of the dipoles in one layer is opposite to that in the other layer [28]. Like the DDI corresponding to parallel dipoles, the DDI corresponding to antiparallel dipoles can be realized by static electric and/or microwave fields. For example, one can apply a static electric field $\mathbf{E}$ and excite the molecules in one layer to rotational states $(J,M) = (1,\pm1)$, which have an effective polarization parallel to $\mathbf{E}$. The molecules in the other layer, preferably a different species with a different rotational constant, can be excited to rotational states $(J,M) = (1,0)$, which are effectively polarized opposite to $\mathbf{E}$. Thus molecules in the same layer are subject to a repulsive DDI at long range, and molecules in different layers are subject to an attractive DDI. Details about the DDI in a static electric field can be found in Ref. [29], where alternative approaches using microwave fields are also worked out.

In this work we study such a bilayer of bosonic dipoles with antiparallel polarization. The key result is that it is a self-bound liquid: unlike a gas, which expands if there are no walls, or a trap potential, which exerts external pressure, a liquid is bound together by the interaction between its particles; hence the interaction must be at least partially attractive. The DDI is clearly partially attractive, depending on the orientations of the dipoles relative to the distance vector between them. However, this is not enough to ensure a self-bound liquid: as mentioned above, dipolar bilayers with the same polarization in both layers undergo dimerization below a certain layer distance [27], yet the system as a whole is not self-bound. We show that the liquid nature is a consequence of the particular form of the interlayer DDI for opposite polarization, which is attractive for finite separation [the two-dimensional (2D) separation projected on the bilayer planes]. This leads to cohesion due to "dipole bridges" that effectively act as a glue to bind all particles together. As required for a liquid, the densities in the bilayers adjust to an equilibrium density $\rho_{\rm eq}$ in the absence of external pressure. $\rho_{\rm eq}$ can be adjusted over a very wide range by the distance d between the layers.

*Corresponding author: robert.zillich@jku.at

For our calculations we use a variational many-body theory, the hypernetted-chain Euler-Lagrange method (HNC-EL), which includes optimized pair correlations. The HNC-EL method has been demonstrated to give accurate results even for such dense and strongly correlated quantum liquids as superfluid ^{4}He. For comparison and validation, we use path-integral Monte Carlo (PIMC) simulations.

II. METHODOLOGY

A 1D optical lattice slices a Bose-Einstein condensate (BEC) into quasi-2D layers separated by a distance d. Since the dipole length r_D can easily exceed the typical d value of about 500 nm, the DDI interaction between dipoles in different layers can lead to appreciable coupling. We consider here two translationally invariant layers A and B, approximate each layer as two-dimensional, and assume no tunneling occurs. With these simplifications we get two coupled 2D systems, i.e., a binary Bose mixture. For simplicity we assume the particles in the two layers have the same mass and dipole moment. As is common in this field, we use dimensionless quantities, where length is given in units of the dipole length r_D and energy is in units of the dipole energy $E_D = \hbar^2/(mr_D^2)$. Other dimensionless quantities follow from r_D and E_D; for example, the number density is given in units of r_D^{-2}, etc. The Hamiltonian in dipole units is

$$H = -\frac{1}{2}\sum_{\alpha,i}\nabla_{i,\alpha}^2 + \frac{1}{2}\sum_{\alpha,\beta}{\sum_{i,j}}' v_{\alpha,\beta}(|\mathbf{r}_{i,\alpha} - \mathbf{r}_{j,\beta}|)\,,$$

where α and β index the layer, $\alpha,\beta \in \{A,B\}$, and i and j index the particles within a layer. The primed sum indicates that for $\alpha = \beta$ we only sum over $i \neq j$. Note that all coordinates $\mathbf{r}_{i,\alpha}$ are 2D projections on the layer plane; the z coordinate is either zero or d in layer A or B, and this d dependence is integrated into the interaction $v_{\alpha,\beta}$. $v_{\alpha,\beta}(|\mathbf{r}_{i,\alpha} - \mathbf{r}_{j,\beta}|)$ is the DDI, in units of E_D, between dipole i at $\mathbf{r}_{i,\alpha}$ in layer α and dipole j at $\mathbf{r}_{j,\beta}$ in layer β. We neglect short-range interactions compared to the DDI. The intralayer interaction ($\alpha = \beta$) is purely repulsive, $v_{\alpha,\alpha}(r) = 1/r^3$. The interlayer interaction, $\alpha \neq \beta$, is $v_{AB}(r) = (2d^2 - r^2)/(d^2 + r^2)^{5/2}$, which is repulsive for small r but attractive for large r and has a minimum at $r_{\min} = 2d$. We show $v_{AA}(r) = v_{BB}(r)$ in Fig. 1 with a solid line and, for layer distances $d = 0.1,\ldots,0.5$, $v_{AB}(r)$ with dashed lines. Although longer ranged, $v_{AB}(r)$ looks qualitatively similar to the interaction between two neutral atoms: an attractive well, followed by repulsion for small r. Note that since the average interlayer interaction vanishes, $\int d^2r\, v_{AB}(r) = 0$, the coupling between layers in the ground state would vanish in a mean-field approximation and the ground-state energy would just be the sum of the energies of each layer.

For the many-body ground state we use the variational Jastrow-Feenberg ansatz [30] consisting of a product of pair-correlation functions for a multicomponent Bose system,

$$\Psi_0 = \exp\left[\frac{1}{4}\sum_{\alpha,\beta}{\sum_{i,j}}' u_{\alpha,\beta}(|\mathbf{r}_{i,\alpha} - \mathbf{r}_{j,\beta}|)\right]. \qquad (1)$$

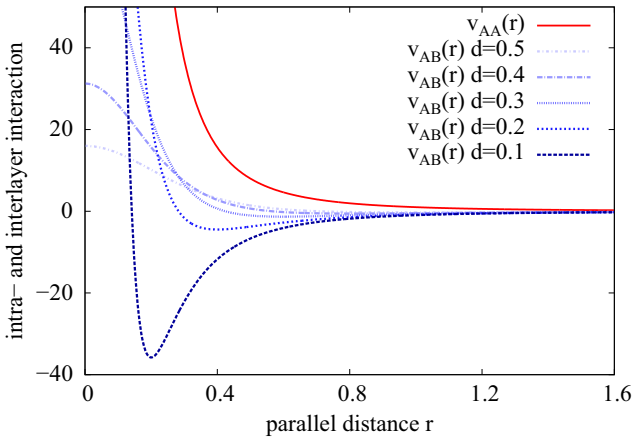

FIG. 1. Intralayer interaction $v_{AA}(r) = v_{BB}(r)$ (solid line) and interlayer interaction $v_{AB}(r)$ (dashed lines) for $d = 0.1,\ldots,0.5$, as a function of the parallel distance, i.e., the distance projected on the layer planes.

Higher-order correlations $u_{\alpha,\beta,\gamma}(\mathbf{r}_{i,\alpha},\mathbf{r}_{j,\beta},\mathbf{r}_{k,\gamma})$ could be included, as is routinely done for single-component calculations. Past experience has shown that triplet correlations improve the ground-state energy, leading to results very close to exact QMC simulations, but they do not change the qualitative picture. We therefore restrict ourselves to pair correlations but check the results against PIMC simulations (details about the PIMC simulations are given in the Appendix). The expression for the expectation value of the energy, $E \equiv \langle\Psi_0|H|\Psi_0\rangle/\langle\Psi_0|\Psi_0\rangle$, contains not only $u_{\alpha,\beta}(r)$ but also the pair distribution function $g_{\alpha,\beta}(r)$, defined as

$$g_{\alpha,\beta}(|\mathbf{r}_\alpha - \mathbf{r}_\beta|) = \frac{N_\alpha(N_\beta - \delta_{\alpha\beta})}{\rho_\alpha\rho_\beta}\int d\tau_{\alpha,\beta}|\Psi_0|^2,$$

where the integral is over all particles except one in layer α and one in layer β and $\rho_\alpha = N_\alpha/V$ is the partial density of component α. $u_{\alpha,\beta}(r)$ and $g_{\alpha,\beta}(r)$ are, of course, related, via the exact hypernetted-chain equations [31],

$$g_{\alpha,\beta}(r) = e^{u_{\alpha,\beta}(r)+N_{\alpha,\beta}(r)+E_{\alpha,\beta}(r)}\,.$$

The sum of all so-called nodal diagrams $N_{\alpha,\beta}(r)$ is itself related to $g_{\alpha,\beta}(r)$ via the multicomponent generalization of the Ornstein-Zernicke relation [31], which would provide closure to the equations were it not for the sum of all "elementary diagrams" $E_{\alpha,\beta}(r)$. The latter can only be computed approximately, e.g., by truncating the sum. Here, we simply neglect them completely; what we said about neglecting triplet correlations also applies to neglecting elementary diagrams.

The pair distributions $g_{\alpha,\beta}(r)$ (and thus the energy and other quantities of interest) are determined from Ritz's variational principle, i.e., from the Euler-Lagrange equations, $\delta E/\delta g_{\alpha,\beta}(r) = 0$. These coupled, nonlinear equations are generically called hypernetted-chain Euler-Lagrange equations and are called HNC-EL/0 if the elementary diagrams are neglected as in the present work. Details about the HNC-EL method can be found in reviews [32,33]. Particularly for Bose mixtures, the HNC-EL/0 equations for an arbitrary number of components can be cast into the following form (bold capital

letters denote matrices; see Refs. [34–37]):

$$\mathbf{W}(k) = -\frac{1}{2}[\mathbf{S}(k)\mathbf{T}(k) + \mathbf{T}(k)\mathbf{S}(k) - 3\mathbf{T}(k) + \mathbf{S}^{-1}(k)\mathbf{T}(k)\mathbf{S}^{-1}(k)],$$

$$V^{ph}_{\alpha,\beta}(r) = g_{\alpha,\beta}(r)v_{\alpha,\beta}(r) + \frac{\hbar^2}{2m_{\alpha,\beta}}|\nabla\sqrt{g_{\alpha,\beta}(r)}|^2 + (g_{\alpha,\beta}(r) - 1)W_{\alpha,\beta}(r),$$

$$\mathbf{V}^{ph}(k) = \mathbf{S}^{-1}(k)\mathbf{T}(k)\mathbf{S}^{-1}(k) - \mathbf{T}(k),$$

where $m_{\alpha,\beta}$ is the reduced mass (for the symmetric bilayer, $\hbar^2/2m_\alpha = \hbar^2/2m_\beta = 1/2$ in dipole units). $S_{\alpha,\beta}(k)$ is the static structure function

$$S_{\alpha,\beta}(k) = \delta_{\alpha\beta} + \sqrt{\rho_\alpha\rho_\beta}\,\mathrm{FT}[g_{\alpha,\beta} - 1],$$

where FT denotes Fourier transformation. The kinetic-energy matrix, $T_{\alpha,\beta}(k) = \delta_{\alpha\beta}(\hbar^2k^2/4m_{\alpha,\beta})$, becomes $T_{\alpha,\beta}(k) = \delta_{\alpha\beta}\frac{k^2}{2}$ in our case. The HNC-EL/0 equations can be solved iteratively. Usually, the convergence is stable and fast, but close to an instability like the spinodal point discussed below, we use linear mixing between iterations to ensure convergence.

III. RESULTS

We calculated the ground-state energy per particle $E(\rho)/N$ as a function of total density $\rho = \rho_A + \rho_B$ for different layer distances d. The interlayer DDI scales with d^{-3}; therefore the energy per particle E/N varies over a wide range, as can be seen in the top panel of Fig. 2, which shows $E(\rho)/N$ for four values of d. A key result is that $E(\rho)/N$ has a minimum at a certain equilibrium density $\rho_{\mathrm{eq}}(d)$, where the pressure p vanishes: without an externally applied pressure provided, e.g., by a radial trap potential, the total density of the bilayer system will adjust itself to $\rho_{\mathrm{eq}}(d)$. Rather than expanding like a gas, a dipolar bilayer system with antiparallel polarization is a *self-bound liquid*. Despite the purely repulsive intralayer interaction, the partly attractive interlayer interaction provides the "glue" that binds the system to a liquid. The phenomenon of an effective intralayer attraction, mediated by particles in the other layer, is discussed in more detail below.

During the iterative numerical optimization, convergence becomes very sensitive as the density ρ or the distance d between layers A and B is decreased, until the HNC-EL/0 equations eventually fail to converge. Past experience with HNC-EL/0 is that a numerical instability usually has a physical reason. Indeed, as we will show below, there is a spinodal point at a d-dependent critical density ρ_{sp} where the homogeneous phase assumed in our calculation becomes unstable against phase separation by nucleation of two-dimensional droplets ("puddles"). Thus the equation of state $E(\rho)/N$ for a *homogeneous* phase can be calculated only for densities $\rho > \rho_{\mathrm{sp}}$. This can be seen in the top panel of Fig. 2, where each curve for $E(\rho)/N$ has an end point. The end point is close to the critical density ρ_{sp} (reaching $\rho = \rho_{\mathrm{sp}}$ is impossible since already an infinitesimal fluctuation can nucleate a finite density wave, creating, e.g., a bubble).

Also shown in the top panel of Fig. 2 are the energies obtained with PIMC simulations (see the Appendix). The temperature for the PIMC simulations is set to $T = 0.5$ ($T = 0.25$ for the smallest ρ), which is low enough that the thermal effect on E/N is smaller than the symbol size. The open triangles are bulk simulations of $N_A = N_B = 50$ dipoles with periodic boundary conditions. The HNC-EL/0 results are upper bounds on E/N, consistent with a variational approach. The overall dependence of E/N on ρ and d is reproduced quite well with the HNC-EL/0 method, which is orders of magnitude faster than PIMC simulations. The black triangle shows the energy from a PIMC simulation of $N_A = N_B = 50$ dipoles and layer separation $d = 0.1$ *without* periodic boundary conditions. Due to the liquid nature of the bilayer, the dipoles in the simulation indeed coalesce into a droplet of finite density, given by $\rho_{\mathrm{eq}}(d)$ apart from corrections due to the surface line tension. The density corresponding to the solid triangle is obtained from the radial density profile $\rho(r)$ at $r = 0$ (see Fig. 7 in the Appendix), where r is defined relative to the center of mass of the droplet. Thermal evaporation, which can occur in the absence of periodic boundary conditions, was suppressed by choosing a much lower temperature of $T = 0.0625$. Although this simulation of a finite cluster is not equivalent to bulk PIMC or HNC-EL/0 calculations, the central density of the droplet is indeed close to $\rho_{\mathrm{eq}}(d)$ from HNC-EL/0.

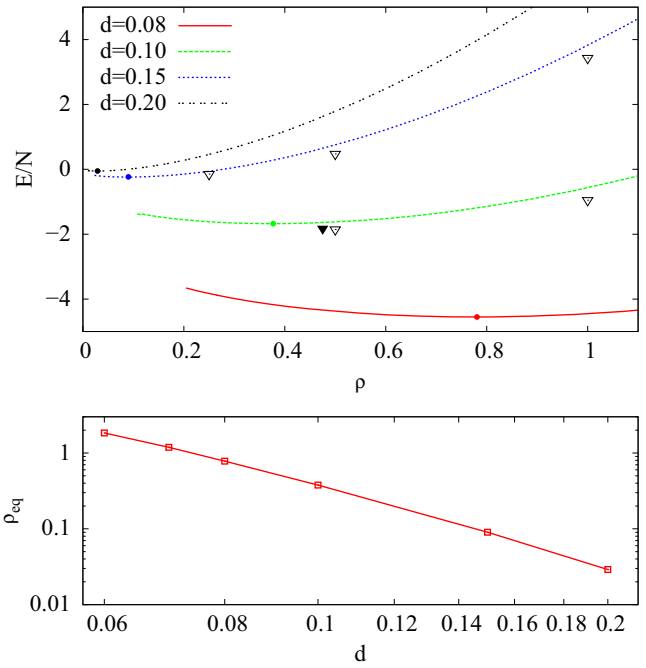

FIG. 2. Top: Ground-state energy per particle E/N versus the total density ρ for several layer distances d. The results from HNC-EL/0 are shown as lines (small circles indicate the equilibrium density ρ_{eq}); the open symbols are from corresponding PIMC simulations. The solid symbol indicates E/N and ρ_{eq} estimated from a PIMC simulation of a self-bound two-dimensional droplet of 50 dipoles in each layer; see the Appendix. Bottom: Equilibrium density ρ_{eq} versus d.

The equilibrium density ρ_{eq} as a function of d is shown in the bottom panel of Fig. 2. $\rho_{\mathrm{eq}}(d)$ decreases rapidly with increasing d. For smaller d, the decrease is approximately $\rho_{\mathrm{eq}} \sim d^{-3}$, and for larger d it is closer to $\rho_{\mathrm{eq}} \sim d^{-4}$. Based purely on the interlayer DDI $v_{AB}(r)$, one would expect a

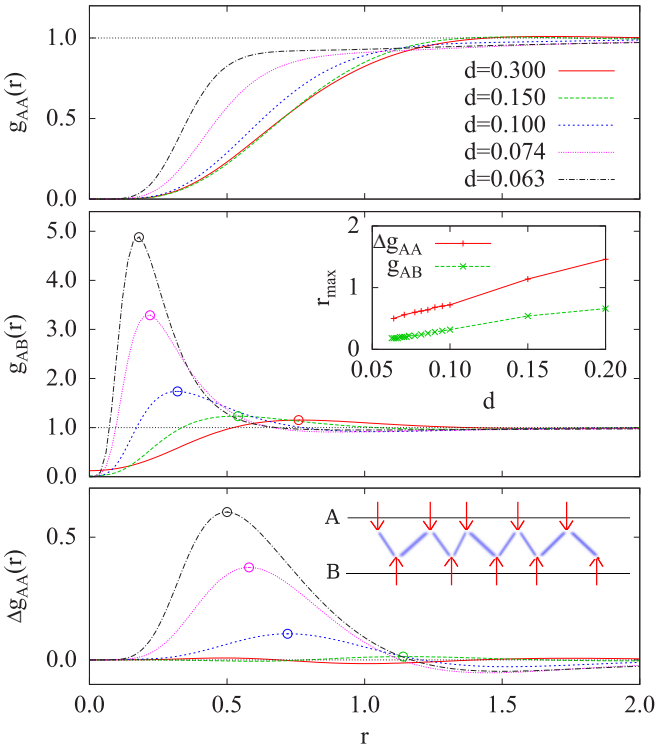

FIG. 3. Top: Intralayer pair distributions $g_{AA}(r)$ at density $\rho_A = \rho_B = 0.5$ for progressively smaller layer distance d. Middle: Corresponding interlayer pair distributions $g_{AB}(r)$, with circle indicating the maxima of $g_{AB}(r)$. Bottom: Incremental intralayer pair distributions $\Delta g_{AA}(r) = g_{AA}(r) - g^{\infty}_{AA}(r)$, i.e., the change from uncoupled layers. The inset in the middle panel shows the positions of the maxima of $g_{AA}(r)$ and $g_{AB}(r)$ as a function of d. The inset in the bottom panel sketches the attractive forces between dipoles in different layers.

scaling of $\rho_{\rm eq}$ with the inverse square of $r_{\rm min} = 2d$, leading to a scaling d^{-2}. The deviation from d^{-2} is due to the kinetic energy. Only for very small d [very deep $v_{AB}(r)$] can this simple picture be expected to be valid, and indeed, the $\rho_{\rm eq}$ curve becomes less steep for smaller d in the double-logarithmic representation in Fig. 2. We note that in the regime of very small d, and thus of extremely strong interlayer correlations, the HNC-EL method would not be reliable anymore.

In Fig. 3 we show the intralayer and interlayer pair distributions, $g_{AA}(r)$ and $g_{AB}(r)$, in the top and middle panels for progressively smaller layer distance d up to the smallest numerically stable value $d = 0.063$ for $\rho = 1$. The growth of a strong-correlation peak in $g_{AB}(r)$ as d is decreased is a direct consequence of the increasingly deep attractive well of $v_{AB}(r)$ around $r_{\rm min} = 2d$ (see Fig. 1). The peak in $g_{AB}(r)$ is located at a distance r_m which is somewhat larger than $2d$ due to zero-point motion. But $g_{AA}(r)$ also develops additional correlations, seen as a shoulder in the top panel. The additional correlations are best seen in the difference between $g_{AA}(r)$ and the uncoupled ($d \to \infty$) limit $g^{\infty}_{AA}(r)$, $\Delta g_{AA}(r) = g_{AA}(r) - g^{\infty}_{AA}(r)$, shown in the bottom panel. The additional positive correlation between dipoles in the *same* layer is mediated by dipoles in the *other* layer: the attraction between a dipole in layer A and a dipole in layer B, which leads to a peak at distance r_m, induces an effective attraction between the dipole in A and another dipole in A, leading to a peak at about twice the distance, $2r_{\rm m}$. The inset in the middle panel shows the positions of the peaks of $g_{AB}(r)$ and $\Delta g_{AA}(r)$ [indicated by circles in the plots of $g_{AB}(r)$ and $\Delta g_{AA}(r)$] as a function of distance d. Indeed, the peaks of $\Delta g_{AA}(r)$ are located at about twice the distance of the peaks of $g_{AB}(r)$. This effective intralayer attraction, induced by the real interlayer attraction, is illustrated by a simple 1D sketch in the inset in the bottom panel, which also illustrates a preference for a certain interparticle spacing, i.e., density, where "dipole bridges" (blue lines in the sketch) can form. The present 2D situation is more complicated than the simple 1D sketch, but our results for the pair correlations demonstrate this picture is approximately valid.

The identification of the low-density instability with a spinodal point can be proven by calculating the long-wavelength modes. For two coupled layers, there are two excitation modes $\epsilon_{1,2}$ for any given wave number k, a density mode and a concentration mode. In the density oscillations, the dipoles in different layers move in phase, and in a concentration oscillation they move out of phase. In the long-wavelength limit, $k \to 0$, each mode can be characterized by the speed of a density or concentration fluctuation, c_1 and c_2, respectively. At the spinodal point, the speed of sound c_1 vanishes, which means that the system becomes unstable against infinitesimal $k \to 0$ fluctuations of the total density, triggering the spinodal decomposition: the system spatially separates into a high-density phase and a low-density phase, such as droplets surrounded by vacuum (at $T = 0$). The easiest way to calculate c_1 and c_2 is the Bijl-Feynman approximation (BFA) for the excitation energies $\epsilon_i(k)$. In the case of a single component, the BFA excitation energy $\epsilon(k)$ follows from $\frac{k^2}{2} = \epsilon(k)S(k)$, which is of course trivial to solve; we get the well-known Bijl-Feynman approximation $\epsilon(k) = \frac{k^2}{2S(k)}$ [38]. In the case of a multicomponent Bose system we need to solve the generalized eigenvalue problem $\frac{k^2}{2}\vec{\phi} = \epsilon_i(k)\mathbf{S}(k)\vec{\phi}$, where $\mathbf{S}(k)$ is the static structure matrix introduced above. For strong correlations, the BFA gives only a rough idea of the true excitation structure; for example, the BFA for the roton energy of superfluid ^{4}He is off by a factor of 2. However, it describes the low-momentum limit of the dispersion relation very well, which is what we need for c_i. For a symmetric bilayer, the eigenvalues are

$$\epsilon_{1,2}(k) = \frac{k^2}{2}[S_{AA}(k) \pm S_{AB}(k)]^{-1},$$

with the associated eigenvectors $\vec{\phi}_1 \sim (1,1)$ and $\vec{\phi}_2 \sim (1,-1)$. $\vec{\phi}_1$ describes fluctuations of the total density, where particles in different layers move in phase, and $\vec{\phi}_2$ describes concentration fluctuations, where particles in different layers move out of phase and the total density is constant. For small k, $\epsilon_1(k) < \epsilon_2(k)$, i.e., the density mode has lower energy than the concentration mode. For $k \to 0$ we get

$$c_{1,2} = \tfrac{1}{2}(S'_{AA} \pm S'_{AB})^{-1}, \qquad (2)$$

with $S'_{\alpha,\beta} = dS_{\alpha,\beta}(k)/dk|_{k=0}$. For single-component Bose systems, it is known that the long-wavelength limit of $S(k)$ obtained with HNC-EL is biased by the approximation made for elementary diagrams (omitted here altogether). This leads to an inconsistency between the speed of sound c obtained from

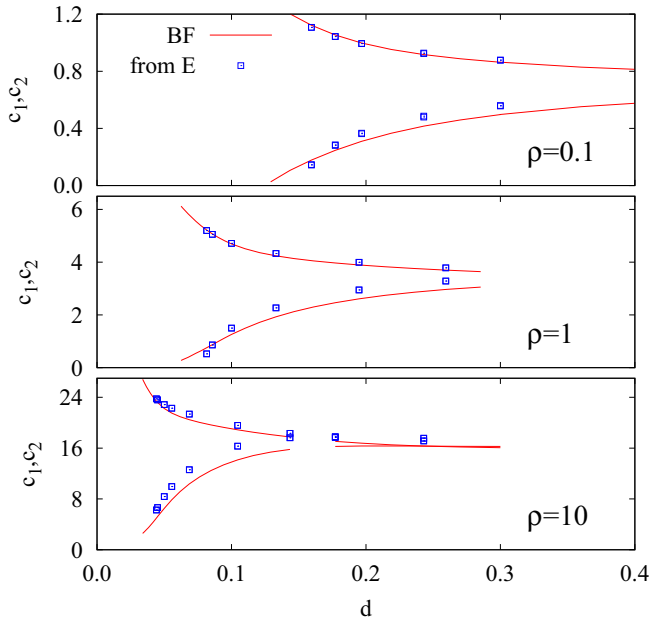

FIG. 4. Speed of density fluctuations c_1 and speed of concentration fluctuations c_2 as a function of layer distance d for three densities, $\rho = 0.1, 1, 10$ (top, middle, and bottom panels). Solid lines show the Bijl-Feynman approximation, Eq. (2), and symbols are the thermodynamic estimates, Eq. (3).

the HNC-EL approximation for $S(k)$ and the thermodynamic relation between c and the energy, $c^2 = \frac{\partial}{\partial\rho}\rho^2\frac{\partial}{\partial\rho}\frac{E}{N}$ (in dipole units). Therefore we need to assess the reliability of our results for c_1 and c_2 in the present case of a multicomponent Bose system. We compare the BFA values obtained from $S_{\alpha,\beta}(k)$, Eq. (2), with the generalization of the thermodynamic relation between $c_{1,2}$ and the energy to binary systems:

$$c_{1,2} = \sqrt{\frac{\rho}{2}(e_{AA} \mp e_{AB})}, \tag{3}$$

where $e_{\alpha\beta}$ is the second derivative of E/N with respect to ρ_α and ρ_β [39].

In Fig. 4 the results for c_1 and c_2 obtained with Eqs. (2) and (3), respectively, are shown as a function of layer distance d for densities $\rho = 0.1, 1, 10$. As the coupling between layers is increased by reducing d, c_1 and c_2 behave differently. The speed of concentration fluctuations c_2 increases (without actually diverging), while the quantity of main interest, the speed of density fluctuations c_1, decreases to zero, in agreement with the interpretation of the instability as a spinodal point. The critical distance where c_1 vanishes is lower for higher ρ. Thus increasing the density for a given d makes the system more stable. The BFAs for $c_{1,2}$ and their thermodynamic estimates agree qualitatively but differ especially for the interesting regime near the spinodal point where $c_1 \to 0$. The Bijl-Feynman values for c_1 appear to go to zero linearly and at slightly smaller d, while the thermodynamic estimates approach zero more steeply, possibly in a nonanalytic fashion. Unfortunately, these uncertainties preclude a meaningful analysis of critical exponents for $c_1(d)$ or $c_1(\rho)$. Monte Carlo simulations, including a finite-size scaling analysis, may shed more light on this question but would certainly require very large simulations, which is beyond the scope of PIMC simulations performed for this paper.

IV. CONCLUSION

We have shown that a dipolar bilayer with antiparallel polarization in the two layers constitutes a *self-bound liquid*, evidenced by a minimum of $E(\rho)/N$ at a finite density $\rho_{\rm eq}$. This means the dipoles in the two layers relax to a stable equilibrium density and require no external pressure provided by a radial trapping potential. This makes it possible to study homogeneous quantum phases because, apart from a narrow surface region, the density is essentially constant and given by $\rho_{\rm eq}$. The value of $\rho_{\rm eq}$ can be controlled by the distance d between the layers (measured in dipolar units), where $\rho_{\rm eq}$ decreases with increasing d. The intra- and interlayer pair distribution functions, $g_{AA}(r)$ and $g_{AB}(r)$, exhibit distinct peaks that show that the liquid can be understood as being held together by a network of "dipole bridges": the attraction between dipoles in different layers mediates an effective attraction between dipoles in the same layer that overcomes the repulsion of the intralayer dipole-dipole interaction. Such situations where an interspecies attraction wins against an intraspecies repulsion are common for self-bound systems. For example, in an ionic crystal the arrangement of having oppositely charged ions as close as possible (nearest neighbors) and equally charged ions farther away (next-nearest neighbors) leads, of course, to stable crystals.

For comparison and validation of our HNC-EL/0 results we performed exact PIMC simulations and found good agreement with our HNC-EL/0 results. Furthermore, and as expected for a liquid, the equation of state $E(\rho)/N$ ends at a critical density $\rho_{\rm sp}$ (*spinodal point*) below which the bilayer becomes unstable against infinitesimal long-wavelength perturbations and breaks into droplets. This is evidenced by a vanishing speed c_1 of total density fluctuations, which we determined from our HNC-EL/0 results using two independent methods, which agree quite well and only deviated from each other very close to the spinodal point. Finite-size PIMC simulations confirm that the system indeed coalesces into a droplet with a flat density profile given by the equilibrium density.

ACKNOWLEDGMENTS

We acknowledge financial support by the Austrian Science Fund FWF (Grant No. 23535) and discussions with F. Mazzanti, J. Boronat, G. Astrakharchik, and W. Lechner.

APPENDIX: PIMC SIMULATIONS

An important question is how accurate our ground-state results obtained with the variational HNC-EL/0 method, where we neglect elementary diagrams and higher than two-body correlations in the ansatz for the wave function [Eq. (1)], are. We performed path-integral Monte Carlo (PIMC) simulations to assess the quality of our HNC-EL/0 results and found good agreement between HNC-EL/0 energies and PIMC energies at low temperature. In this appendix we present additional comparisons of the static structure matrix, as well as results for finite systems, where self-bound "puddles," i.e., 2D droplets, are formed because of the spinodal instability. All simulations

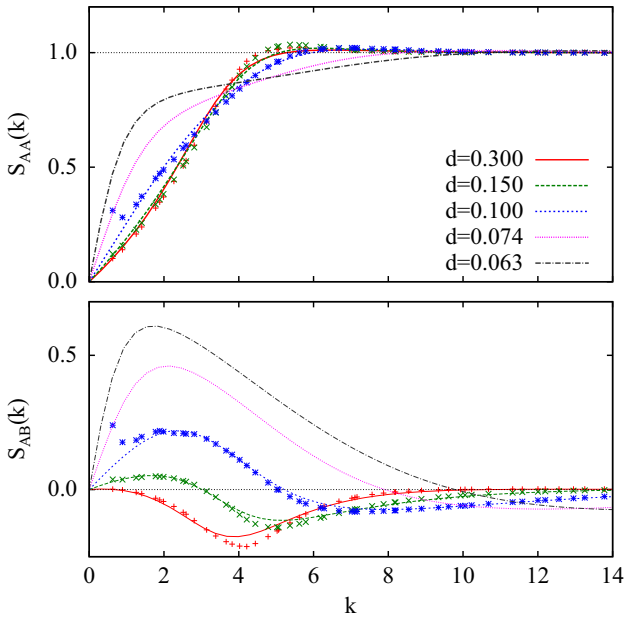

FIG. 5. Static structure functions $S_{AA}(k)$ (top) and $S_{AB}(k)$ (bottom) obtained with HNC-EL/0 (lines) for a total density $\rho = 1$ and progressively smaller layer distances d as indicated in the top panel. The symbols show $S_{AA}(k)$ and $S_{AB}(k)$ obtained by PIMC simulations at $T = 0.5$ for distances down to $d = 0.1$.

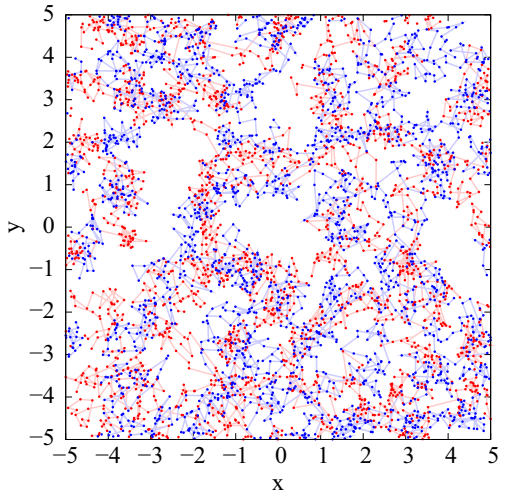

FIG. 6. PIMC simulations snapshot for $\rho = 1$ and $d = 0.1$ ($T = 0.5$). Red (light gray) and blue (dark gray) chains are the dipoles in layers A and B.

were done with 50 particles per layer; bulk simulations used quadratic simulation boxes with periodic boundary conditions with a box size adjusted to achieve a given density. For antiparallel bilayers, cutoff corrections to the dipole-dipole interaction cancel each other and therefore are not needed.

For predicting the spinodal instability and also for calculating excitation properties, an important quantity is the static structure matrix $S_{\alpha\beta}(k)$. In Fig. 5 we compare $S_{AA}(k)$ and $S_{AB}(k)$ obtained with HNC-EL/0 (lines) and PIMC (symbols) at a total density of $\rho = 1$. The temperature in the PIMC simulation was $T = 0.5$, which was low enough that $S_{\alpha\beta}(k)$ did not change upon lowering the temperature further. We see that the HNC-EL/0 approximation works well, considering that intralayer correlations are quite strong. For $d = 0.3$ and $d = 0.15$ PIMC simulations predict slightly more pronounced peaks and troughs, but HNC-EL/0 calculations are faster by several orders of magnitude. For $d = 0.1$, the agreement is also very good, except for the smallest k value possible in a simulation box of side length 10, $k = 2\pi/10 \approx 0.63$. In the PIMC results, both $S_{AA}(k)$ and $S_{AB}(k)$ turn up sharply for this smallest k value. When we reduce d even more, this apparent peak at $k = 0$ grows very large. This peak has a very simple reason: as we approach the spinodal point by reducing d, we enter the metastable regime of the phase diagram, where E/N as a function of total density has a negative slope. In this regime a finite perturbation can lead to a collapse, and the system phase separates. Since PIMC has no trial wave function that could prevent phase separation, this collapse indeed happens as we go further below the equilibrium density. In fact, Monte Carlo snapshots such as in Fig. 6 show density fluctuations already for $d = 0.1$ that resemble small "bubbles," i.e., voids in the liquid dipolar bilayer. In Fig. 6 red (light gray) and blue (dark gray) dots, connected by lines, are the beads of the discretized imaginary-time paths sampled in PIMC; each bead is a particle at a discrete time step. For even lower d or lower total densities we observe a clear decomposition into a droplet and a low-density gas, as discussed in the next paragraph. A large peak at $k = 0$ can therefore be seen as a zero-momentum Bragg peak due to phase separation.

As final confirmation of the liquid nature of dipolar bilayers with antiparallel polarization, we show the results of a PIMC simulation without periodic boundary conditions. Since there is no radial trapping potential, a two-dimensional gas would, of course, spread out indefinitely. A liquid, on the other hand, will coalesce into a droplet of finite density. For a droplet that is

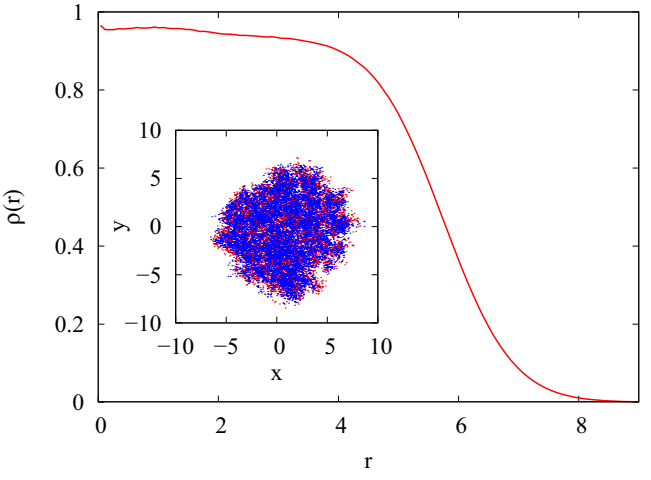

FIG. 7. Density profile $\rho(r)$ for a self-bound droplet of 50 dipoles in each layer. Inside the droplet the density is approximately constant, with a value close to the equilibrium density ρ_{eq} of a bulk system at zero pressure. The distance is $d = 0.1$, and the temperature was set to $T = 0.0625$, which is low enough to prevent evaporation. The inset shows a snapshot of the simulation, with red (light gray) and blue (dark gray) indicating the dipoles in layers A and B, respectively, at the imaginary time steps of the paths of PIMC.

large enough that effects of surface line tension are negligible, the density inside the droplet is given by the equilibrium density ρ_{eq}, i.e., the density of a bulk system at zero pressure. In Fig. 7 we show the radial density profile $\rho(r)$ for 50 dipoles in each layer separated by $d = 0.1$, where r is measured relative to the center of mass. In order to prevent evaporation we set the temperature to $T = 0.0625$. $\rho(r)$ is approximately constant for $r \lesssim 4$ and quickly falls to zero for larger r. This is the behavior expected for the density profile of a self-bound liquid and very different from the density profile of a quantum gas in a trap. As discussed above and shown in Fig. 2, indeed, $\rho(r = 0) \approx \rho_{eq}$ even for such a small droplet.

[1] A. Griesmaier, J. Werner, S. Hensler, J. Stuhler, and T. Pfau, Phys. Rev. Lett. **94**, 160401 (2005).
[2] T. Lahaye, T. Koch, B. Fröhlich, M. Fattori, J. Metz, A. Griesmaier, S. Giovanazzi, and T. Pfau, Nature (London) **448**, 672 (2007).
[3] M. Lu, N. Q. Burdick, S. H. Youn, and B. L. Lev, Phys. Rev. Lett. **107**, 190401 (2011).
[4] K. Aikawa, A. Frisch, M. Mark, S. Baier, A. Rietzler, R. Grimm, and F. Ferlaino, Phys. Rev. Lett. **108**, 210401 (2012).
[5] M. A. Baranov, Phys. Rep. **464**, 71 (2008).
[6] T. Lahaye, C. Menotti, L. Santos, M. Lewenstein, and T. Pfau, Rep. Prog. Phys. **72**, 126401 (2009).
[7] M. A. Baranov, M. Dalmonte, G. Pupillo, and P. Zoller, Chem. Rev. **112**, 5012 (2012).
[8] J. Deiglmayr, A. Grochola, M. Repp, K. Mörtlbauer, C. Glück, J. Lange, O. Dulieu, R. Wester, and M. Weidemüller, Phys. Rev. Lett. **101**, 133004 (2008).
[9] K.-K. Ni, S. Ospelkaus, M. H. G. de Miranda, A. Pe'er, B. Neyenhuis, J. J. Zirbel, S. Kotochigova, P. S. Julienne, D. S. Jin, and J. Ye, Science **322**, 231 (2008).
[10] K. Aikawa, D. Akamatsu, M. Hayashi, K. Oasa, J. Kobayashi, P. Naidon, T. Kishimoto, M. Ueda, and S. Inouye, Phys. Rev. Lett. **105**, 203001 (2010).
[11] J. M. Sage, S. Sainis, T. Bergeman, and D. DeMille, Phys. Rev. Lett. **94**, 203001 (2005).
[12] T. Takekoshi, M. Debatin, R. Rameshan, F. Ferlaino, R. Grimm, H.-C. Nägerl, C. R. Le Sueur, J. M. Hutson, P. S. Julienne, S. Kotochigova, and E. Tiemann, Phys. Rev. A **85**, 032506 (2012).
[13] G. Bismut, B. Laburthe-Tolra, E. Marechal, P. Pedri, O. Gorceix, and L. Vernac, Phys. Rev. Lett. **109**, 155302 (2012).
[14] C. Ticknor, R. M. Wilson, and J. L. Bohn, Phys. Rev. Lett. **106**, 065301 (2011).
[15] L. Santos, G. V. Shlyapnikov, and M. Lewenstein, Phys. Rev. Lett. **90**, 250403 (2003).
[16] D. H. J. O'Dell, S. Giovanazzi, and G. Kurizki, Phys. Rev. Lett. **90**, 110402 (2003).
[17] D. Hufnagl, E. Krotscheck, and R. E. Zillich, J. Low Temp. Phys. **158**, 85 (2010).
[18] D. Hufnagl, R. Kaltseis, V. Apaja, and R. E. Zillich, Phys. Rev. Lett. **107**, 065303 (2011).
[19] D. Hufnagl and R. E. Zillich, Phys. Rev. A **87**, 033624 (2013).
[20] A. Macia, F. Mazzanti, J. Boronat, and R. E. Zillich, Phys. Rev. A **84**, 033625 (2011).
[21] A. Macia, D. Hufnagl, F. Mazzanti, J. Boronat, and R. E. Zillich, Phys. Rev. Lett. **109**, 235307 (2012).
[22] G. E. Astrakharchik, J. Boronat, I. L. Kurbakov, and Y. E. Lozovik, Phys. Rev. Lett. **98**, 060405 (2007).
[23] H. P. Buchler, E. Demler, M. Lukin, A. Micheli, N. Prokofev, G. Pupillo, and P. Zoller, Phys. Rev. Lett. **98**, 060404 (2007).
[24] N. Matveeva and S. Giorgini, Phys. Rev. Lett. **109**, 200401 (2012).
[25] S. Moroni and M. Boninsegni, Phys. Rev. Lett. **113**, 240407 (2014).
[26] F. Deuretzbacher, G. M. Bruun, C. J. Pethick, M. Jona-Lasinio, S. M. Reimann, and L. Santos, Phys. Rev. A **88**, 033611 (2013).
[27] A. Macia, G. E. Astrakharchik, F. Mazzanti, S. Giorgini, and J. Boronat, Phys. Rev. A **90**, 043623 (2014).
[28] W. Lechner and P. Zoller, Phys. Rev. Lett. **111**, 185306 (2013).
[29] A. Micheli, G. Pupillo, H. P. Büchler, and P. Zoller, Phys. Rev. A **76**, 043604 (2007).
[30] E. Feenberg, *Theory of Quantum Fluids* (Academic, New York, 1969).
[31] J. P. Hansen and I. R. McDonald, *Theory of Simple Liquids* (Academic, New York, 1976).
[32] E. Krotscheck, in *Microscopic Quantum Many-Body Theories and Their Applications*, edited by J. Navarro and A. Polls, Lecture Notes in Physics Vol. 510 (Springer, Berlin, 1998), pp. 187–250.
[33] E. Krotscheck and M. Saarela, Phys. Rep. **232**, 1 (1993).
[34] K. E. Kürten and C. E. Campbell, Phys. Rev. B **26**, 124 (1982).
[35] C. E. Campbell, Ann. Phys. (N.Y.) **74**, 43 (1972).
[36] T. Chakraborty, Phys. Rev. B **26**, 6131 (1982).
[37] M. Hebenstreit, B.S. thesis, Johannes Kepler University, 2013.
[38] R. P. Feynman, Phys. Rev. **91**, 1291 (1953).
[39] C. E. Campbell, J. Low Temp. Phys. **4**, 433 (1971).